Cyclic convection in a zone bounded by stable layers

Murshed Hossain and D. J. Mullan
Bartol Research Institute, University of Delaware, Newark, Delaware 19716
(Received 9 February 1996; revised manuscript received 21 June 1996)

We have simulated compressible convection in two distinct but related cases: (i) a single layer of unstable material is in contact with impenetrable boundaries and (ii) a layer of unstable material that is identical to that of case (i) except that it is now ''sandwiched'' between two thick stable layers. The convection is driven equally strongly in both cases. We find that convection in the single layer is steady, whereas in the ''sandwich'' case, the convection exhibits nonsteady behavior of a particular kind: the convection is cyclic. During one part of the cycle, the convective flux F_C falls to levels that are too small for energy balance. During the second part of the cycle, conduction increases in an attempt to restore energy, but this eventually drives the fluid back to convective instability, with a subsequent increase in F_C. In the course of the cycle, the fluctuations in F_C are large (factors of 2–3). We comment on the applicability of our results to convection in the sun. [S1063-651X(97)05003-4]

PACS number(s): 47.27.−i

I. INTRODUCTION

The properties of convective flows in a convectively unstable fluid are determined by a number of factors, including the mechanical and thermal characteristics of the fluid, the boundary conditions, and how strongly the convection is being driven. Studies of convection in laboratory conditions typically involve (a) nearly incompressible fluid, (b) impenetrable boundaries with prescribed temperatures, and (c) levels of driving that range from only slightly supercritical to strong. We are interested in simulations of convection in the sun. The differences between conditions in the solar convection zone and in the laboratory are considerable: in the sun we must allow for (a) highly compressible fluid, (b) completely penetrable ''boundaries'' with ill-defined positions and temperatures, and (c) strong driving. Because of these differences, it is possible that certain features of astrophysical convection have no analog in the laboratory case. In this paper we explore one such feature, namely, heat transport that cycles back and forth between convection and conduction.

In order to relate our work to other simulations of convection (both laboratory and astrophysical), we first highlight some of the stages that convection theory has gone through.

A. Assumptions in convection modeling

In the earliest analysis of convective instability by Rayleigh [1], the aim was to explain Benard's [2] experimental results for the onset of convection in a liquid. There are five assumptions that typically enter into analysis of Rayleigh-Benard (RB) convection: (i) the Boussinesq approximation (i.e., the fluid is treated as incompressible except for slight density fluctuations associated with thermal expansion, with constant coefficient α); (ii) the linear regime; (iii) prescribed boundary temperatures; (iv) the depth-independent kinematic viscosity ν and thermal diffusivity $\kappa=K/\rho C_p$ (where K is thermal conductivity, ρ is density, and C_p is specific heat); and (v) impenetrable boundaries at well-defined spatial locations, separated by vertical distance ζ. In the incompressible case, $\kappa=$const (equivalent to $K=$const) leads to the result that the temperature gradient $|dT/dz|\equiv\beta_0$ in thermal equilibrium is depth independent. (The subscript 0 denotes parameters in the equilibrium state.) In terms of the parameter $\mathrm{Ra}=g\alpha\beta_0\zeta^4/\kappa\nu$ (where g is the acceleration due to gravity), Rayleigh [1] showed that convection occurs only if the driving is sufficiently strong, i.e., only if Ra exceeds $\mathrm{Ra}_{\mathrm{crit}}=27\pi^4/4\approx 660$. In the next five paragraphs we summarize some of the salient changes that emerge when we relax each of the five assumptions of RB convection, (i)–(v) above.

Relaxing the assumption of incompressibility, Spiegel [3] estimated $\mathrm{Ra}_{\mathrm{crit}}$ for a perfect gas (where pressure p is given by $p=R\rho T$ and R is the gas constant). In this case, in the limit of constant conductivity, the equilibrium state still has $\beta_0=$const, but the density and pressure profiles in the equilibrium state are no longer linear functions of z: instead the condition of hydrostatic equilibrium requires that the depth dependences be $\rho_0\sim z^m$ and $p_0\sim z^{m+1}$, where the ''polytropic index'' m is not arbitrary but depends on the temperature gradient β_0 according to $m=g/R\beta_0-1$. [We shall use this relation in dimensionless form below (Sec. II B).] When the material is compressible, it is no longer the absolute value of the temperature gradient $|\beta_0|$ that is relevant in estimating the strength of convective driving: instead, the relevant quantity in the expression for Ra is now the superadiabaticity, i.e., the excess of $|\beta_0|$ over the adiabatic gradient $|\beta_{\mathrm{ad}}|=g/C_p$ [4]. Now, for a perfect nonionizing gas, $C_p=2.5R$: in the dimensionless units that we use below in our equations, $R=1$, and this leads to $(dT/dz)_{\mathrm{ad}}=g/2.5$. With the above definition of m, this means that a configuration with $m>$ ($<$) 1.5 is stable (unstable) to convection in the dissipationless limit. When one evaluates $\mathrm{Ra}_{\mathrm{crit}}$ in the compressible case, one finds that in the limit where the temperatures at the bottom and top are almost equal $T_b/T_t\rightarrow 1$ (i.e., nearly incompressible), $\mathrm{Ra}_{\mathrm{crit}}$ approaches the incompressible value ($\sim$600); but for large T_b/T_t, $\mathrm{Ra}_{\mathrm{crit}}$ in a perfect gas is greatly reduced, to values as small as $\sim$53 for $T_b/T_t=11$ [5].

Relaxing the linear assumption of RB convection, laboratory studies [6] have shown that nonlinear convective flows can achieve a steady state provided that the driving is not too strong ($\mathrm{Ra}/\mathrm{Ra}_{\mathrm{crit}} \leqslant 10-20$). In the limit of strong driving, the flows become turbulent [6]. In the case of compressible convection, the nonlinear regime exhibits subsonic flows when the driving is not too strong, shocks may form in strongly driven flows [7], and convective cells have vertical extents comparable to the local scale height [8,9]. In the present paper, we are interested in time-dependent behavior of a cyclic nature: since turbulence might mask the time behavior we are studying, we choose cases where the driving is not so strong as to lead to turbulence.

Relaxing the RB assumption of prescribed temperatures on the boundaries, astrophysical convection is typically simulated *not* by specifying the *temperature* on both boundaries, but by specifying the *heat flux input* on the bottom boundary and the temperature at the top [10]. This set of boundary conditions is very different from that which is typically used in laboratory conditions: in the laboratory, with fixed temperatures at top and bottom, there are no constraints on the heat flux. As a result, the heat flux that is carried by conduction F_{cond} may be small compared to the flux that is eventually transported by convection F_C. The Nusselt number $\mathrm{Nu}=F_C/F_{\mathrm{cond}}$ may therefore be large in such conditions. In contrast to this, if we apply the boundary condition that a certain flux is inputted at the bottom boundary, then to achieve thermal equilibrium in the initial configuration, the thermal conductivity cannot be arbitrarily small: as a result, even when convection is fully developed, Nu remains very modest: $\mathrm{Nu} \leqslant 2.5/(m+1)$ [17]. For example, in a case where $m=1$, the maximum value of Nu is found to be no more than 1.25 [11].

Relaxing the RB assumption regarding depth independence, the diffusivities can be given significant depth dependences. In such cases, the evaluation of criteria for the onset of convection requires numerical integration [12]. The values of $\mathrm{Ra}_{\mathrm{crit}}$ in some cases are several orders of magnitude smaller than Rayleigh's original number.

Finally, in an attempt to allow for the fact that astrophysical convection includes no material boundaries, the RB assumption concerning impenetrable boundaries can be relaxed by placing layers of stable compressible gas above and below the unstable layer [13]. For brevity, we refer to this configuration as a ''sandwich.'' A schematic illustration of a sandwich can be seen by referring to Fig. 4 below, although Fig. 4 as such is not strictly applicable to the sandwich case. The relevant point here is that we are looking at fluid in the x-z plane, with z being vertical. The fluid is 6 units of length deep and 2π units of length wide. At time $t=0$, convectively unstable fluid is confined to the region where arrows are plotted in Fig. 4. In the case that we refer to as the ''one-layer configuration'' (see Sec. II C below), the convectively unstable fluid is bounded above and below by impenetrable walls. In the sandwich case, the impenetrable walls are moved to $z=0$ and 6 and the ''blank'' areas above and below the ''arrowed'' region in Fig. 4 are occupied by stable gas in immediate contact with the unstable gas. The temperature is fixed at $T=1$ at the top and the heat flux is prescribed at the bottom. As time progresses, convective flows develop in the unstable gas and some of these overshoot into the stable fluid above or below. The thicker the stable layers of the sandwich the smaller the flow speeds when overshooting plumes reach the computational boundaries: in this context the relevant thickness of the layers is measured in terms of the contrast in density and/or pressure from top to bottom. In terms of density scale height $H_d=dz/d\ln\rho$ or pressure scale height $H_p=dz/d\ln p$, the convectively unstable layer is effectively isolated from (nonphysical) boundary effects if the stable layers are several scale heights thick.

B. Astrophysical convection

Convection zones in solarlike stars are bounded above and below by layers of stable gas. Therefore, if we can determine the properties of convection in a sandwich configuration, it may assist in interpreting certain features of astrophysical convection.

Several previous numerical simulations of compressible convection in configurations where unstable gas is in contact with one or two stable layers have been reported [11,13–16]. The principal emphasis in those investigations was to address the question: how does convection (specifically, overshooting) affect the adjacent stable gas?

The emphasis of our work is the inverse of that in Refs. [11,13–16]. Here our aim is to address the following question: how does the presence of adjacent stable gas affect convection in the unstable layer?

C. The focus of this paper

To achieve our aim, a key aspect of our work is a comparison and contrast of two carefully controlled simulations. The first (the one-layer case) contains an unstable layer of compressible gas in contact with impenetrable boundaries. The second contains the identical unstable layer as in the first case, except that now the layer is sandwiched between thick layers of stable compressible gas above and below.

In both cases, the same heat fluxes are inputted at the bottom boundary, the same temperatures are assigned initially to the top boundary, the same depth dependences are assigned to the diffusivities, and the same driving strengths $\mathrm{Ra}/\mathrm{Ra}_{\mathrm{crit}}$ are assigned to the initial states. By choosing conditions in this way, our aim is to isolate and identify those effects that are due to the presence or absence of impenetrable boundaries.

The equations and methods we use in our simulations are outlined in Sec. II. We present our results in Sec. III and the discussion is in Sec. IV. We conclude in Sec. V.

II. EQUATIONS AND METHODS

The conservation equations of mass, momentum, and energy can be expressed in the nondimensional form [8,9,12,17]

$$\frac{\partial \rho}{\partial t}+\frac{\partial}{\partial x_j}(\rho v_j)=0, \tag{1}$$

$$\frac{\partial v_i}{\partial t}+v_j\frac{\partial v_i}{\partial x_j}=-\frac{1}{\gamma\rho}\frac{\partial p}{\partial x_i}+\frac{1}{\rho\,\mathrm{Re}}\frac{\partial \sigma_{ij}}{\partial x_j}+g, \tag{2}$$

$$\frac{\partial p}{\partial t}=-v_j\frac{\partial p}{\partial x_j}-\gamma p\frac{\partial v_j}{\partial x_j}+(\gamma-1)\frac{\gamma}{\mathrm{Re}}\sigma_{kj}\frac{\partial v_k}{\partial x_j}+\frac{\gamma}{\mathrm{Pe}}\frac{\partial}{\partial x_j}\left[K\frac{\partial}{\partial x_j}\left(\frac{p}{\rho}\right)\right]. \tag{3}$$

The equation of state is that of a perfect gas: in nondimensional units, this is given by

$$p=\rho T. \tag{4}$$

In Eqs. (1)–(3), t is the time and x_j,v_j are the components of direction and velocity vector, respectively, with z vertically upward. g is the (constant) vertically downward gravity. γ is the ratio of specific heats: we take it to be constant and equal to $\frac{5}{3}$ in this work. σ_{ij} is the viscous stress tensor.

In Eqs. (1)–(3), T, p, and ρ are expressed in units of their respective values at the top of our computational domain, T_t, p_t, and ρ_t. The velocities are scaled in units of the adiabatic sound speed at the top $c_t=(\gamma p_t/\rho_t)^{1/2}$. Our unit of length L_0 is defined to be such that the width of the horizontal domain is equal to $2\pi L_0$ and the depth of the domain is $z_{\max}L_0$. For all runs reported here, we choose $z_{\max}=6$. Time is measured in sound-crossing units L_0/c_t at the top of the domain. In these units, gravity g_i is expressed in units of c_t^2/L_0; σ_{ij} is in units of $\mu_t c_t/L_0$, where μ_t is the dynamic viscosity at the top. Conductivity K is in units of the conductivity at the top K_t.

When fluid equations are integrated, the level of dissipation in any particular run is prescribed by assigning numerical values to any two among a set of four dimensionless numbers: the Rayleigh number, the Prandtl number, the Reynolds number, and the Péclet number. In material that is incompressible, one frequently has at least an order of magnitude estimate of the mean flow speed U_m: it is typically the speed that is imposed on the flow. Moreover, one also has some knowledge of the length scale L over which flow variables change appreciably: this allows one to define a Reynolds number or a Péclet number in terms of U_m, e.g., $\mathrm{Re}=U_mL/\nu$ and $\mathrm{Pe}=U_mL/\kappa$. However, when we deal with thermal convection, the mean flow speed is unknown and cannot be assigned a value beforehand: the flow speed is part of the solution that we must obtain by integrating the equations. Therefore, we are forced to define Re and Pe in terms of a speed other than the flow speed: since we are dealing with compressible material, the natural unit of speed in the problem is the sound speed. As a result, we choose the following definitions for the two dimensionless parameters that control the amount of dissipation in our compressible flows:

$$\mathrm{Re}=\frac{\rho_t L_0 c_t}{\mu_t}, \tag{5}$$

$$\mathrm{Pe}=\frac{\rho_t L_0 c_t C_p}{K_t}. \tag{6}$$

Note that $\mathrm{Re}/c_t\sim 1/\nu_t$, where ν_t is the kinematic viscosity at the top, and $\mathrm{Pe}/c_t\sim 1/\kappa_t$, where κ_t is the thermal diffusivity at the top. Thus the product of our two dissipation numbers $\mathrm{Re}\times\mathrm{Pe}/c_t^2$ scales as $1/\kappa_t\nu_t$: this combination of parameters appears in the original definition of the Rayleigh number Ra (see Sec. I A above), indicating that once the dissipation parameters Re and Pe are chosen, Ra is no longer an independent parameter. The product Re×Pe will also appear below when we define a ''dynamic'' Rayleigh number to characterize our flows [see Eq. (8) below]. We solve the equations as an initial boundary value problem on a two-dimensional grid of size $N_x\times N_z$.

A. Boundary conditions

In the horizontal directions, the boundary conditions are periodic. In the one-layer case, unstable gas is in contact with impenetrable stress-free walls at top and bottom. On the top wall the temperature is specified and on the bottom wall the heat flux is specified.

In the sandwich case, a convectively unstable layer with identical thermal and mechanical properties to those in the one-layer configuration is placed with a stable layer on top (several H_p thick) and a stable layer underneath [$(1–2)H_p$ thick]. Ideally, the thicker the stable layers, the more isolated the unstable layer from boundary effects: the values we choose here are a computational compromise, and we shall see below (Sec. IV E) that as long as the stable layers are thicker than about $0.7H_p$, this suffices to isolate the convective flows from boundary effects. The top and bottom boundaries of the computational domain are stress-free impenetrable walls with the same thermal boundary conditions as in the one-layer case.

B. Initial conditions: Sandwich convection

For the sandwich simulations, we want $|dT/dz|$ in the center of the domain to be steep enough so as to be convectively unstable, while near the top and bottom, $|dT/dz|$ should be shallow enough to ensure convective stability. In the interest of eliminating numerical artifacts from the solutions as much as possible, we avoid the use of piecewise continuous expressions: we prefer to use an analytic function for the temperature profile. The expression that we chose for $T(z)$ is

$$T(z)=T_0+a\,\ln[(z-z_0)+\sqrt{(z-z_0)^2+1}]. \tag{7}$$

Here z_0, the location of steepest gradient, is chosen near the center of the domain and T_0 is given a value there. Once z_0 and T_0 are given, a is assigned a (negative) value such that at the top $T\to 1$. In the runs to be reported below, we chose $z_0=3.4$ and $T_0=3.6$. With these choices, $a=-1.544$. The bottom temperature in this case is $T_b=6.6$. The temperature profile $T(z)$ with this choice of parameters is shown by the solid curve in Fig. 1. The profile of the adiabatic gradient T_{ad} is shown in Fig. 1 by the dashed line: the slope of this line is $-6/5$, corresponding to our choice of $g=-3.0$ (see below). Compressible material is convectively stable (unstable) in regions where the slope of the solid line in Fig. 1 is steeper than the slope of the dashed line, i.e., $|dT/dz|<(>)\ |dT/dz|_{\mathrm{ad}}$. Visual inspection of Fig. 1 shows that the slope of the solid curve is shallower than adiabatic near the bottom ($z=0$) and also near the top ($z=6$), while at intermediate depths, there is a portion of the solid curve that has a steeper slope than the dashed curve.

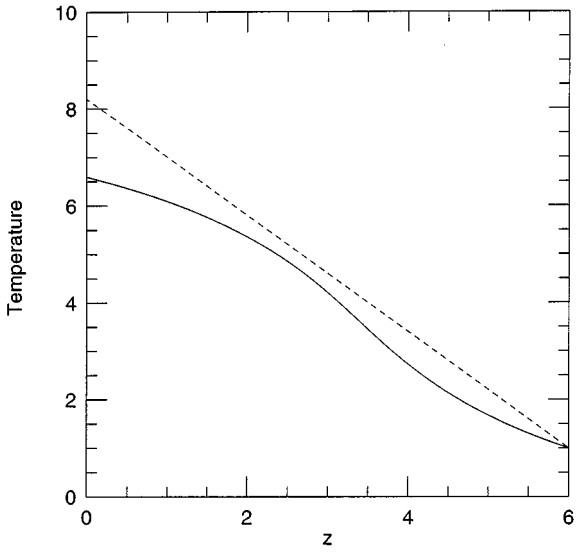

FIG. 1. Solid curve, dimensionless temperature profile $T(z)$ in the initial configuration; dashed line, adiabatic temperature profile.

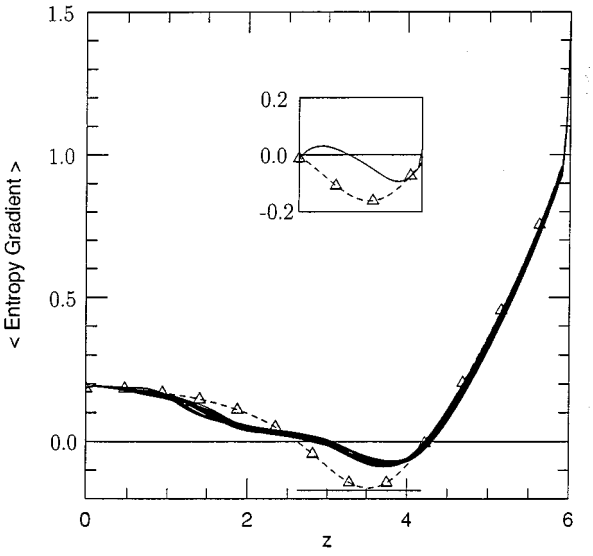

FIG. 2. Dashed line and open triangles, dimensionless entropy gradient dS/dz as a function of vertical coordinate in the initial sandwich model. Stable layers $dS/dz>0$ exist at the top and bottom: an unstable layer $dS/dz<0$ lies between the two stable layers. Solid lines, profiles of dS/dz when the flows are in the nonlinear regime; inset, profiles of dS/dz in simulation of one-layer convection; dashed line, initial profile; solid line, profile in nonlinear regime.

To make this visual impression more quantitative, we note that, once the temperature profile is chosen, the depth dependence of the polytropic index m follows from the prescription given in Sec. I A above: $m=(g/[dT/dz])-1$ (where g is a negative number in our notation). Given the temperature profile $T(z)$, the initial pressure profile is computed by integrating the hydrostatic relation $dp/dz=\rho g$ downward from the top (where $p_t=1$ and $\rho_t=1$) using the equation of state (4). The absolute value of g and the profile of m combine to determine the pressure contrast across the domain. In the runs reported below, with $g=-3.0$, the pressure contrast is 492. In this case, the polytropic index m has the value 4.4 at the top, 5.9 at the bottom, and has a minimum of 0.943 near the middle of the unstable layer. As was mentioned above, $m<1.5$ suffices for convective instability in the material we consider (a perfect, nonionizing gas). Once a value is assigned to g, the adiabatic temperature gradient $(dT/dz)_{\rm adiab}$ is obtained from $(dT/dz)_{\rm adiab}=g/2.5$: this is the equation for the dashed line in Fig. 1 (with $T=1$ at the top).

The plot of temperature profiles in Fig. 1 is not the only way to illustrate where stability and instability occur. An alternative approach is provided by considering the entropy $S\sim\ln(p/\rho^{\gamma})$. In an adiabatic process, $S=$const. Therefore, at locations where $dS/dz<0$ (>0), the material is convectively unstable (stable). In Fig. 2, open triangles joined by a dashed line indicate the vertical gradient of entropy dS/dz (horizontally averaged) in the initial configuration. (The continuous lines will be discussed below.) Note that the values of dS/dz are positive near the top and near the bottom, indicating that the fluid there is convectively stable. However, dS/dz is negative (i.e., the fluid is convectively unstable) at intermediate depths (Fig. 2). Note that the dashed profile in Fig. 2 is in hydrostatic equilibrium. The thermal conductivity is given a z-dependent value such that the conductive heat flux is constant at all depths.

Across the upper stable region ($z\approx4.2$–6), the pressure varies by a factor of 30–40. Thus, in terms of local pressure scale height H_p, the upper stable layer is $\sim4H_p$ thick. The unstable region extends from $z_{\rm UB}\approx2.6$ to $z_{\rm UT}\approx4.2$, corresponding to the horizontal bar near the lower boundary of Fig. 2: the extent of this bar is 1–2 times the local H_p. The thickness of the lower stable region ($z\approx0$–2.6) also corresponds to 1–2 times the local H_p.

C. Initial conditions: One-layer configuration

In the one-layer configuration, we choose only the portion of the above temperature profile that is unstable, i.e., we consider only the fluid that lies between $z_{\rm UB}$ and $z_{\rm UT}$ and place an impenetrable wall at each of these depths. In this case, $N_x\times N_z=64\times34$. At heights between $z_{\rm UB}$ and $z_{\rm UT}$ the initial temperature profile and the initial entropy profile are chosen to be identical to the profiles that we use in the sandwich case. The inset in Fig. 2 illustrates dS/dz for the one-layer case: the horizontal positioning of the inset is such that the range of z values in the inset is aligned with the range of z values that are unstable in the sandwich case (see the horizontal bar near the bottom of Fig. 2). The dashed line with triangles in the inset is the initial profile of dS/dz and is identical to the corresponding portion of the dashed line in the main part of Fig. 2. In the inset, the initial dS/dz is entirely negative, i.e., convective instability extends throughout the domain and convective flows come in contact with impenetrable walls at top and bottom. This corresponds to a one-layer configuration similar to the ones that have been studied in the literature [5,8].

III. RESULTS

To initiate flows we impose a small vertical velocity in the domain. The equations are then integrated in time for

many hundreds of sound crossing times. In the one-layer configuration, convection rolls develop (see Fig. 4), and these become steady in time. In the sandwich case, the convective flows that develop are time dependent and overshoot into the overlying and underlying stable fluids. In order to describe our results, it is helpful first to introduce a parameter that essentially extends the concept of the Rayleigh number (well known in linear stability theory) into the nonlinear regime.

A. Dynamic Rayleigh number

Ever since Rayleigh's [1] work, it has been traditional to characterize the convective stability properties of a container of depth d in terms of the Rayleigh number $\mathrm{Ra}=g(1/\kappa\nu)d^4|\beta|\alpha$: the ordering of the terms in this expression is chosen for ease of comparison with Eq. (8) below. The above definition of Ra is a static one and Ra is evaluated at a particular depth (so that $\alpha=1/T$ can be specified) and at a particular time ($t=0$). However, in the present case, a static definition is of limited value: neither the depth of the convective layer nor the value of β is fixed in time, nor is β independent of depth at any time (even at $t=0$). As a result, there is no unique way to define ''the'' traditional Rayleigh number in the present case.

In the present work, in order to have a parameter that describes the convective stability properties of the sandwich case, we choose to define an instantaneous ''dynamic mean Rayleigh number'' Ra_d at time t as

$$\mathrm{Ra}_d(t)=|g_i|\left(\frac{\mathrm{Re}\times\mathrm{Pe}}{c_t^2}\right)d_{\mathrm{eff}}^4(t)\left\langle\frac{|\beta(t)|}{T(t)}\right\rangle_{\mathrm{global}}. \qquad (8)$$

The analogy with the traditional definition of Ra is apparent: the terms $\mathrm{Re}\times\mathrm{Pe}/c_t^2$ in Eq. (8) corresponds to the terms $1/\kappa\nu$ in Ra [see the discussion following Eq. (6) above] and the terms $|\beta|\alpha$ in Ra appear as $|\beta|/T$ inside the angular brackets in Eq. (8). In the limit $m=\mathrm{const}$ and $dT/dz=\mathrm{const}$, Ra_d as defined in Eq. (8) reduces to the original definition by Rayleigh [1] (since $\alpha=1/T$ for a perfect gas). The angular brackets with the subscript global denote an instantaneous spatial average over *all* sites in the domain where the temperature gradient is superadiabatic at time t. Because Eq. (8) includes information at all superadiabatic sites in the domain, the parameter Ra_d allows us to characterize the convective stability properties of the domain in a *global* manner. In particular, it is important to note that we are *not* restricting our considerations to a single horizontal plane, but rather *we are averaging over every point in the domain where the temperature gradient is instantaneously superadiabatic.* The quantity $d_{\mathrm{eff}}(t)$ represents a crude attempt to characterize the instantaneous depth of unstable fluid: it is obtained by evaluating the instantaneous $\beta(t)$ at each site in the grid (using second-order centered finite differences), counting the number of sites N_p at which the temperature gradient is superadiabatic, and then defining d_{eff} as $d\times N_p/(N_x\times N_z)$, where d is the depth of the computational domain. In our runs, d_{eff} turns out to have values that are close to the original choice for the depth of the unstable layer: in units of L_0, d_{eff} turns out to have values of about 1.3 (see Fig. 2). The global average that we use in obtaining a numerical value for Ra_d means that pointwise information is smoothed out in Ra_d; however, there are no drastic differences in the behavior of the convection over an x-y plane. As a result, the unstable layer with $d_{\mathrm{eff}}\approx(1.3\text{–}1.4)L_0$ in the nonlinear phases occupies 20–25 % of the computational domain. We recognize that a more formal definition might be useful, but in the present study, the above definition of Ra_d serves our purposes adequately.

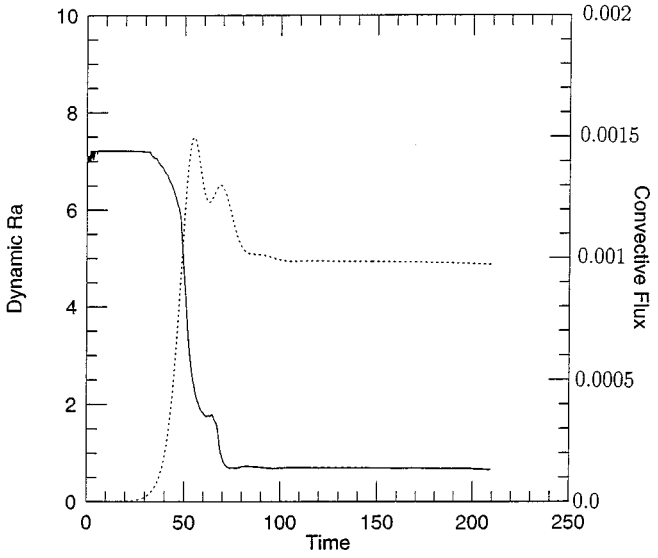

FIG. 3. One-layer convection: time histories of dynamic Rayleigh number Ra_d [defined in Eq. (8)] (solid line) and dimensionless convective flux [defined in Eq. (9)] (dashed line). The units of time are the sound crossing time.

B. One-layer configuration

The one-layer simulation was started from initial conditions such that $\mathrm{Ra}_d(t=0)/\mathrm{Ra}_{\mathrm{crit}}\approx 44$. [The value of $\mathrm{Ra}_{\mathrm{crit}}$ for the prescribed $T(z)$ was determined numerically using the same time-dependent approach that we used in our previous work [12,17].] The time history of Ra_d is shown as a solid line in Fig. 3: the initial relatively large value is maintained up to times of some 30–40 sound crossing times. Then, the convective flows begin to enter a nonlinear regime where the maximum velocities grow rapidly. To quantify the convective heat flux, we consider *a globally averaged quantity*

$$F_C(t)=\frac{\int_{z_{\mathrm{UB}}}^{z_{\mathrm{UT}}}\langle\rho v_z\Delta T\rangle_{\mathrm{hor}}dz}{z_{\mathrm{UT}}-z_{\mathrm{UB}}}. \qquad (9)$$

In the integrand, v_z is the instantaneous vertical velocity and ΔT is the difference between the instantaneous temperature at time t and the initial temperature at the same location. Angular brackets with the subscript hor indicate averages over a horizontal plane at time t. Integration over z allows us to average over the unstable zone in the vertical direction. By taking the global average in Eq. (9) over all heights between the bottom of the unstable layer z_{UB} and the top of the unstable layer z_{UT}, we are allowing for the fact that, at different instants in time, the convective flux may peak at different horizontal levels within the convection zone. The time dependence of F_C is shown by the dashed curve in Fig. 3.

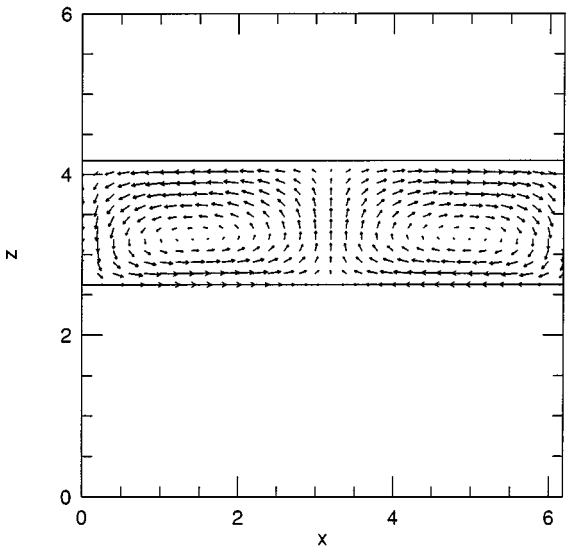

FIG. 4. Snapshot of velocity vectors in one-layer convection.

Although we could, in principle, express F_C in terms of a Nusselt number, this is not especially relevant with the present boundary conditions (see Sec. I A above.)

As the convective flows develop, F_C enters a phase of rapid growth (in the time interval $t=40$–60: see the dashed curve in Fig. 3). During the time interval when F_C is rising to its maximum, it is obvious from Fig. 3 that there is a precipitous drop in the value of Ra_d. After a couple of small oscillations, the system adjusts to what is clearly a steady state: for times in excess of $t\approx100$, both Ra_d and F_C in Fig. 3 remain invariant. The value of Ra_d in this steady state is smaller than the initial value by a factor of more than 10: the flows have caused the mean temperature gradient to approach closer to marginal stability by an order of magnitude.

When steady state is achieved, the entropy gradient dS/dz has the z profile shown by the solid line in the inset in Fig. 2. The solid line shows that dS/dz still remains negative from $z=3.2$ to 4.2: thus convective instability persists over this range of depths. There is also a narrow region of depths from $z=2.6$ to 2.7, where dS/dz is also still negative: this is the lower boundary layer that remains convectively unstable. For the intermediate range of depths ($z=2.7$–3.2), dS/dz is positive. (The presence of an extended region of positive dS/dz in a convection zone with an impenetrable wall at the top has also been pointed out in [18].) Fluid in this intermediate region has become formally stable to convection because nonlinear interactions tend to drive the system toward stability. However, flows that are being driven by the upper and lower unstable boundary regions have enough instability to maintain fluid motions in the formally stable zone. To illustrate this, the velocity vectors in a steady state are shown in Fig. 4: the figure shows convection rolls extending from the top to the bottom of the convective layer (in agreement with the simulation results in [5,10]). Maximum velocities in the flow are 0.52 in our dimensionless units (i.e., Mach number relative to c_t).

Although it is not immediately apparent, there are actually several profiles of dS/dz plotted with solid lines in Fig. 2 (inset): they are ''snapshots'' taken from various instants of time in a steady state. However, they are so similar to each other that our graphics resolution cannot separate them. This is a good indication of the steadiness of the flow regime that has been established.

We can summarize this subsection as follows: our simulations are consistent with empirical results that show that when a convectively unstable fluid is in contact with impenetrable boundaries, the convective flows *can* achieve a steady state provided that the driving is not too supercritical [6]. Our simulations are also consistent with previous simulations [5,8].

C. Sandwich convection

In Fig. 5(a) we show time histories of Ra_d (solid line) and F_C (dashed line) in a simulation of sandwich convection with $\mathrm{Re}=10$ and $\mathrm{Pe}=2$. In Fig. 5(a) it is important to note that we choose the strength of the convective driving to be as close as possible to that in the one-layer case, i.e., the initial Rayleigh number $\mathrm{Ra}_d(t=0)$ in Fig. 5(a) is as close as we can make it (within the constraints set by the discreteness of the grid) to the $\mathrm{Ra}_d(t=0)$ value in Fig. 3. Despite our careful choice of the same initial parameters in Figs. 3 and 5(a), the results for the sandwich configuration are qualitatively quite different from the one-layer case: the initial stage of large (and constant) Ra_d persists for only $\sim$20 time units. Now, the convective flux rises to its first maximum at $t\approx30$, causing $dT/dz\rightarrow dT/dz_{\mathrm{adiab}}$ because of the nonlinear interactions. This corresponds to a precipitous drop in Ra_d. In this case, there are no boundary regions to prevent dT/dz from becoming very close to, or even falling below (in absolute value), dT/dz_{adiab}. The lack of such control has the effect that part of the initially unstable layer *becomes convectively stable*, i.e., the unstable region becomes somewhat narrower. To illustrate this narrowing of the unstable region, we plot the profile of dS/dz at about a dozen instants in Fig. 2 (solid lines). The separate profiles are slightly different from one another, giving the impression of a broad black curve in the figure: close inspection, however, will reveal that there are many individual profiles superposed, and they cycle back and forth as time progresses.

Following the initial precipitous drop in Ra_d, the numerical values of Ra_d and F_C both exhibit behavior that to the eye appears rather cyclic, with a period of about 30–40 dimensionless units. F_C cycles back and forth between ''high'' and ''low'' states. The fluctuations in F_C in the course of the cycle are by no means small: F_C is some 2–3 times larger in the high state than in the low state. The numerical values of Ra_d oscillate above and below a mean value of $\mathrm{Ra}_{dm}\approx2$. To quantify the period of the oscillation, we computed power spectra (not shown) for the time profiles of F_C and Ra_d: maximum power indeed occurs at the period of 33 in dimensionless units, consistent with what the eye picks out in Fig. 5(a).

As regards the temporal behavior of the cycles in Ra_d and F_C in Fig. 5(a), we draw the reader's attention to a clear phase relationship between the cycles. Inspection of Fig. 5(a) indicates that there is a 90° phase shift between the two quantities: when Ra_d reaches an extremum, F_C reaches an extremum in its first time derivative and vice versa.

In the initial state, the unstable regions extended from $z_{\mathrm{UB}}=2.6$ to $z_{\mathrm{UT}}=4.2$ (see the dashed profile in Fig. 2). However, at later times, dS/dz is negative only over a more re-

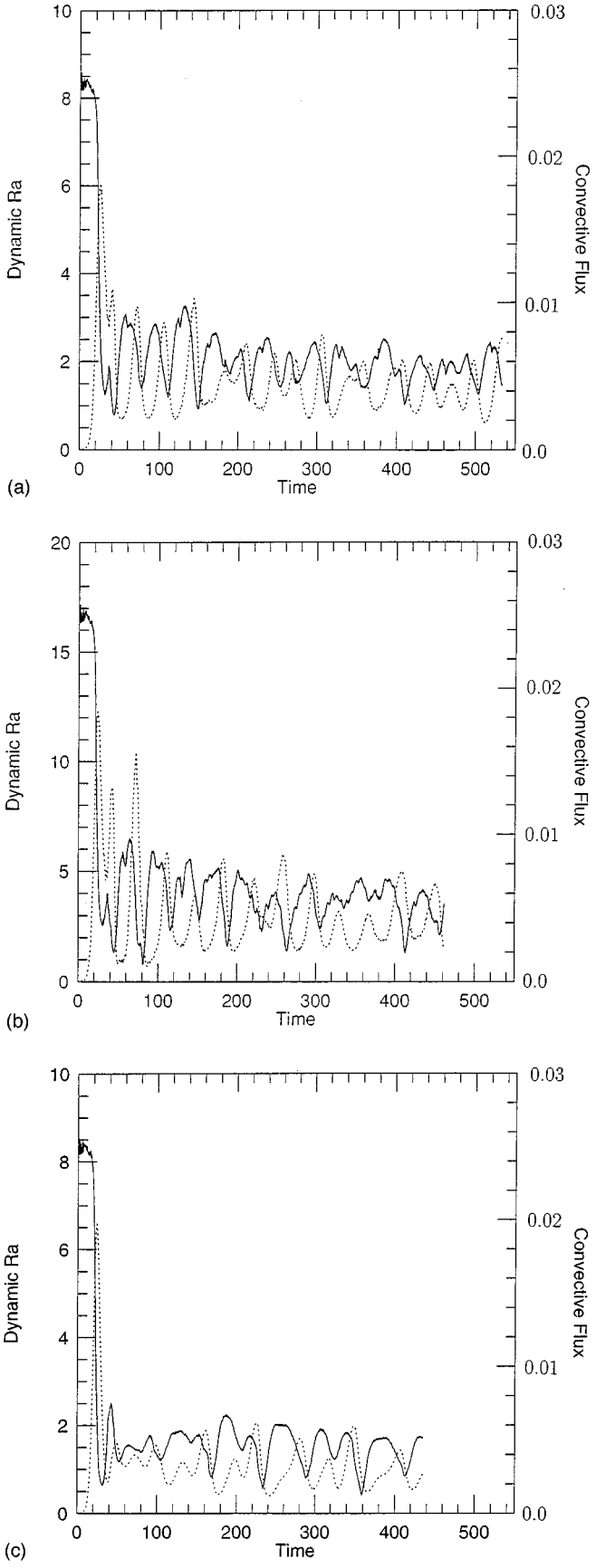

FIG. 5. Sandwich convection: time histories of dynamic Rayleigh number Ra_d (solid line) and dimensionless convective flux (dashed line). (a) Re=10, Pe=2; (b) Re=20, Pe=2; (c) Re=5, Pe=4.

stricted range of z (Fig. 2). The lower part of the initially unstable layer has been eroded by the tendency towards stability, and there is no compensating effect of a lower boundary layer: the unstable region now has a bottom boundary at $z_{\mathrm{UB}} \approx 2.9$–$3.0$. To be sure, the upper regions of the initially unstable layer have also encroached upon the overlying stable layer slightly ($z_{\mathrm{UT}} \approx 4.3$): but this is not as large an effect as what has happened at the lower boundary. The overall effect is for the unstable layer to be now somewhat thinner than initially. Moreover, the thickness of the unstable layer oscillates about its new mean value.

In order to increase the strength of the driving, we increased Re by a factor of 2 to Re=20, but kept Pe=2. Results are shown in Fig. 5(b). Again, cyclic behavior is evident, with a period of about 35 units, almost the same as that in Fig. 5(a). However, in Fig. 5(b), the values of Ra_d oscillate above and below a mean value of $\mathrm{Ra}_{dm} \approx 4$, which is about twice as large as the corresponding number in Fig. 5(a). Finally, in order to investigate the dependence on the Péclet number, we show a run for Pe=4 in Fig. 5(c): in this run, we set Re=5. Now the predominant period in the cycle is about twice as long as before: the power spectra peak at periods of 60–62. Moreover, the values of Ra_d now oscillate around a mean level $\mathrm{Ra}_{dm} \approx 1$. We return to these results below in our discussions of scalings (Sec. IV C).

IV. DISCUSSION

The contrast between the one-layer case and the three-layer (sandwich) case is striking: in the one-layer case, the convection is steady, but in the sandwich case, it is cyclic.

A. Steady convection in a single layer

The temporal behavior in the one-layer simulation can be understood in a straightforward way. Initially, dT/dz is steep enough so that conduction carries all of the flux that is inputted at the lower boundary. However, the temperature profile is highly unstable and Ra_d is large. Because of the instability, convection begins. On time scales of tens of sound crossing times, there is a sharp increase in the heat flux transported by convection F_C. As the convective flux increases, dT/dz throughout *most* of the fluid flattens, approaching the marginally stable (adiabatic) gradient dT/dz_{adiab}. As $dT/dz \rightarrow dT/dz_{\mathrm{adiab}}$, $|\beta| \rightarrow 0$. The more flux convection carries, the less burden is on conduction and so the shallower the temperature gradient can become. The value of Ra_d (as we have defined it) therefore drops: the rate of decline in Ra_d is steepest when F_C is maximum. As Ra_d decreases, i.e., as $|\beta|$ decreases, the tendency for convection to be driven near the center of the domain declines: as a result, F_C falls off from its maximum value. However, although *most* of the fluid is tending towards adiabatic conditions, this is *not* true of two key regions in the flow: the thermal boundary layers at the top and bottom remain convectively unstable and they continue to drive the convection throughout the interior of the convective domain. Because of the accessibility of these unstable layers, the convective flows in the main body of the convection zone do not stop, but can continue to be driven. The steady-state nature of the flows is apparent in the late stages of Fig. 3.

It is the essence of the one-layer case that the fluid throughout the domain has direct access to unstable boundary layers at the top and bottom. Scalings that have been derived for turbulent RB convection in order to explain empirical results [19] depend explicitly on mixing of the material between the unstable boundary layers and the main body of the fluid. These scalings are rather successful in reproducing the empirical results, where values of Ra as high as 10^{14} have been achieved in Boussinesq conditions.

B. Cyclic convection in the sandwich

In the simulation of sandwich convection with equally strong driving, as $dT/dz \rightarrow dT/dz_{\text{adiab}}$, the unstable layer is unable to carry much convective flux. (Note that, because the amount of dissipation in the runs is chosen to be finite, $|dT/dz|$ need not fall below $|dT/dz|_{\text{adiab}}$ for convection to be choked off.) As a result, F_C declines, and the convection looks as if it may ''shut down.'' In this case, because of the adjacent stable layers, *the convection zone has essentially no contact with any unstable boundary layer fluid for driving*. However, as less and less flux is carried by convection, the energy equation demands that conduction begin to carry more and more. Therefore, $|dT/dz|$ must increase to allow conduction to transport most of the flux inserted into the domain at the base. The increase in $|dT/dz|$ causes Ra_d to increase again, the convective flux builds up, and the demands on conduction become less severe. This sets up a cycle.

No steady state is reached: each time convective flux reaches a maximum value, Ra_d undergoes its most rapid rate of decline, and every time F_C reaches a minimum, Ra_d experiences its most rapid rate of increase. The conductive and convective fluxes behave as a sort of flip-flop oscillator in which no steady state exists.

C. Origin of the cyclic behavior

The (pseudo)period of 30–40 units for the cycles in Figs. 5(a) and 5(b) is controlled by a balance between the forces that drive convection and the forces that drive thermal conduction. The convective forces (which tend to make the temperature gradient adiabatic causing Ra_d to fall towards zero) can be characterized by a time scale τ_{adiab} that is expected to scale as $1/\gamma_c$, where γ_c is the growth rate of the fastest growing convective mode. The value of γ_c is controlled by the strength of the convective driving Ra: for the incompressible case, Rayleigh [1] found $\gamma_c \leqslant |\beta_0| \alpha g d^2/(\kappa+\nu)$ [see Eq. (49) in [1]]. In the compressible case, $|\beta_0|$ must be replaced by the superadiabatic excess (the quantity $|\beta|$ in the definition of Ra_d) and $\alpha = 1/T$: the combination $|\beta| g/T$ occurs in our definition of Ra_d [Eq. (8)]. With an aspect ratio of order unity in our case, Rayleigh's scaling for the growth rate becomes (in our dimensionless units) $\tau_{\text{adiab}} \geqslant d_{\text{eff}}^2([\text{Re}+\text{Pe}]/\text{Ra}_d)$.

As regards conduction, the appropriate time scale is $\tau_{\text{cond}} \approx L^2/\kappa$, where L is the dimension of the region over which the conductive heat transport must operate: in our case, with an unstable layer of vertical thickness $d_{\text{eff}} = (1.3\text{–}1.4)L_0$ and horizontal extent $6L_0$, typical values of L might be in the range $(2\text{–}3)L_0$. In terms of the Péclet number [Eq. (5)], this means $\tau_{\text{cond}} \approx \text{Pe}(L/L_0)^2 L_0/c_t$. In our dimensionless units (where one unit of time equals L_0/c_t), this leads to $\tau_{\text{cond}} \approx \text{Pe}(L/L_0)^2$.

In the course of a cycle, convection first sets in because Ra_d is large and therefore the growth times for the convective modes $1/\gamma_c$ are quite short. But as convection develops, the temperature gradient falls so close to adiabatic that $\text{Ra}_d \rightarrow 0$: when this happens, the convective growth times $\tau_{\text{adiab}} \sim 1/\gamma_c \geqslant \text{Ra}_d^{-1}$ become very long. Eventually, τ_{adiab} becomes longer than τ_{cond}: at this point, energy transport becomes dominated by conduction. As a result, the temperature gradient begins to steepen in order to carry the flux that is inserted at the lower boundary. The time scale for this steepening is τ_{cond}: with Pe=2 [as in Figs. 5(a) and 5(b)] and $L/L_0 \approx 2\text{–}3$, τ_{cond} is predicted to be of order 10–20 in our units. This is about one-half of the cycle times in Fig. 5(a) and is consistent with the rise times of the cycles.

As the temperature gradient steepens, Ra_d increases and the convective time scales become shorter: when they fall below τ_{cond} convection takes over the energy transport and the cycle begins anew. The cycle occurs because Ra_d oscillates above and below a mean asymptotic level Ra_{dm} at which the convective growth time $\tau_{\text{adiab}} \geqslant (\text{Re}+\text{Pe})/\text{Ra}_{dm}$ is comparable to τ_{cond}. To see that this is the case in Fig. 5(a), note that $\text{Ra}_{dm} \approx 2$: since Re=10 and Pe=2 in this case [see the caption of Fig. 5(a)], this means that $\tau_{\text{adiab}} \geqslant 6 d_{\text{eff}}^2$, and since $d_{\text{eff}} \approx 1.4$ (in our units), this leads to $\tau_{\text{adiab}} \geqslant 12$. Indeed, the time scales of declining portions of the F_C cycles in Fig. 5(a) are of order 10–20 units of time. The shape of the cycles in Fig. 5(a) is roughly symmetric in time, suggesting that the flow conditions have adjusted in such a way that *convective and conductive time scales tend to be comparable during the course of the cycle*.

This analysis suggests that it is *conduction* effects that control the *period* of the oscillation, whereas it is *convection* effects that control the limiting mean value of Ra_d. The flows adjust themselves so that the dynamic Rayleigh number Ra_d has an asymptotic mean value Ra_{dm} such that the *convective* growth time scale becomes comparable to the *conductive* time scale.

To test that the scalings are as suggested here, we refer to Fig. 5(b), where Pe is unchanged from Fig. 5(a). If the cycle time scale is controlled by the conduction time scale (as we have suggested above), then since the conduction time scale depends on Pe but not on Re, we would expect to see the same period in Figs. 5(a) and 5(b). This is consistent with what we see. However, the increase in Re+Pe by a factor of about 2 (from 12 to 22) in going from Fig. 5(a) to Fig. 5(b) suggests that, if we are to keep the convective time scale $\sim(\text{Re}+\text{Pe})/\text{Ra}_{dm}$ fixed at the same value as before, the asymptotic mean Ra_{dm} about which the cycle will oscillate should increase by a factor of about 2. In fact, it can be seen in Fig. 5(b) that at long times, Ra_d oscillates about a value of about 4, i.e., indeed higher by a factor of about 2 than in Fig. 5(a). Finally, in a run with Pe=4 and Re=5 [Fig. 5(c)], we expect to see a thermal conduction period about twice as long as with Pe=2: in fact, the predominant period in Fig. 5(c) is 60–65, i.e., about twice as long as in Figs. 5(a) or 5(b). In Fig. 5(c), with Re+Pe now having a value of 9 [i.e., close to its value in Fig. 5(a)], a doubling of the convective growth time in Fig. 5(c) relative to that in Fig. 5(a) can be achieved by reducing Ra_{dm} by a factor of about 2 in Fig. 5(c)

compared to Fig. 5(a). In fact, we see that Ra_{dm} in Fig. 5(c) settles down to values of about 1, i.e., a factor of about 2 smaller than Ra_{dm} in Fig. 5(a). Thus the scalings we derived above seem consistent with the numerical results.

D. Contrast with time dependence due to turbulence

The cyclic behavior that we describe here is only one possible form of time dependence that may occur in convective flows. For example, it is well known (e.g., [6,19]) that time-dependent convection can be caused by setting $\mathrm{Ra}_d(t=0)$ in excess of some value: in such cases, the driving may be so strong that the flows become turbulent. However, in such cases, the temporal variations in F_C and Ra_d (if there are any) would probably be controlled by turbulent processes: because of the nature of turbulence, we might not expect to see a clearly defined phase relationship between F_C and Ra_d in strongly forced convection.

In the present paper, we have explored a mechanism that causes convection to become time dependent for quite different reasons: we have chosen the driving to be not so strong that turbulence occurs. In fact, we have been careful to choose driving of such a strength that we can demonstrate that the convective flows are steady in the case where impenetrable boundaries are in direct contact with the convection: then, with exactly the same amount of driving, we have found cyclic behavior in the sandwich configuration. Thus the time dependence we describe here has nothing to do with that which appears in a turbulent flow. In the cyclic case, the flows exhibit a definite phase relationship between F_C and Ra_d. The existence of this phase relationship might provide us with a means to determine whether the time dependence in a particular convective flow is due to boundary conditions (as in the cases reported here) or to a high degree of supercriticality.

E. Penetrative convection

In our simulations, we see the effects of penetrative convection in the lower stable layer: a snapshot of the velocity vectors for the sandwich configuration is shown in Fig. 6. We see downward plumes extending as much as $0.7H_p$ into the stable layer: there are also g modes in the stable layer with frequencies comparable to the local Brunt-Vaisala frequency $\nu_{\mathrm{BF}}=\sqrt{g\alpha\beta}$, which are excited by these plumes. The fact that our simulations contain g modes in the stable fluid is in agreement with previous simulations [10]. The presence of oscillations at ν_{BF} in a stable fluid adjacent to a convectively unstable fluid has also recently been reported in a laboratory experiment [20] where convection is driven in an unusual mode (using horizontal temperature differences).

The length of the overshooting plumes allows us to address the following question: does the transition from one-layer to sandwich convection occur for arbitrarily thin upper and lower stable layers or is there a critical thickness above which these heat flux cycles set in? If we were to choose stable layers that were thinner than $0.7H_p$, then some (or all) of the overshooting plumes would ''sense'' the presence of the impenetrable boundary at the edge of our computational domain. In such cases, the convection would have access to the same boundary layers that play such a key role in determining the properties of convection in the one-layer case. It

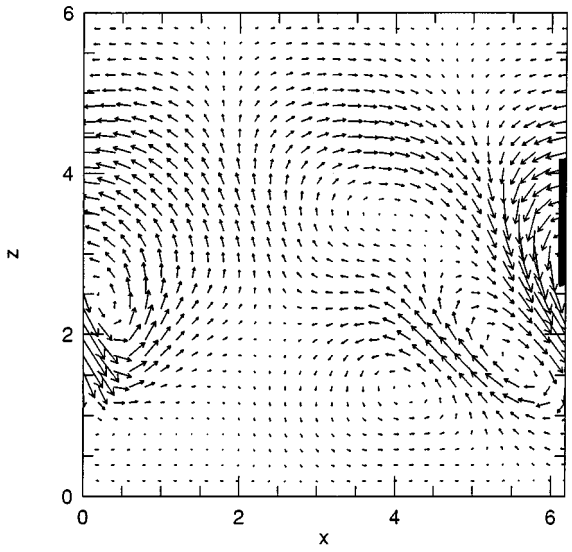

FIG. 6. Snapshot of velocity vectors in the two-dimensional sandwich. The vertical black bar along the right-hand side denotes the initial location of the unstable convection zone.

is our contention in this paper that it is precisely the *lack of access to convectively unstable boundary layers* that allows the convection to enter the cyclic regime. Therefore, we suggest that as long as the stable layers are thicker than $0.7H_p$, cyclic convection becomes possible.

F. Applicability to convection in the sun

We suggest that our results may be applicable to solar convection, where convection occurs in a sandwich configuration, with convectively stable material above and below.

1. Fluctuations in solar flux

Let us consider our result that F_C exhibits large fluctuations (of order unity) in the course of a cycle. It is important to note that the computational domain that we used for our simulations is not large enough to accommodate more than 1–2 convective cells. If a larger domain were used, including N cells, we expect that the amplitude of the fluctuations in F_C would be reduced by factors of order $\sqrt{N}$. If we could run a domain with $N=10^6$ cells [i.e., the number of convection cells (granules) on the surface of the sun], we expect that the fractional fluctuations in F_C would be reduced below what we find $[O(1)]$ to $O(10^{-3})$. The flux of energy from the sun ($F_S \approx 1367\ \mathrm{W\,m^{-2}}$) is known to exhibit temporal fluctuations with amplitudes up to 1–2 $\mathrm{W\,m^{-2}}$ [21]. The largest negative excursions can be ascribed to sunspots, but the data also contain fluctuations that cannot be ascribed to sunspots, and these can also be of order 10^{-3} of the mean value. We note the coincidence with our estimates of convective flux amplitude.

2. Time scales of solar variations

We have argued that the time scale for cyclic convection is controlled essentially by conductive processes. In the sun, conduction is dominated by radiative effects. When therefore we raise the following question: on what time scale does convection in the sun cycle back and forth between high and

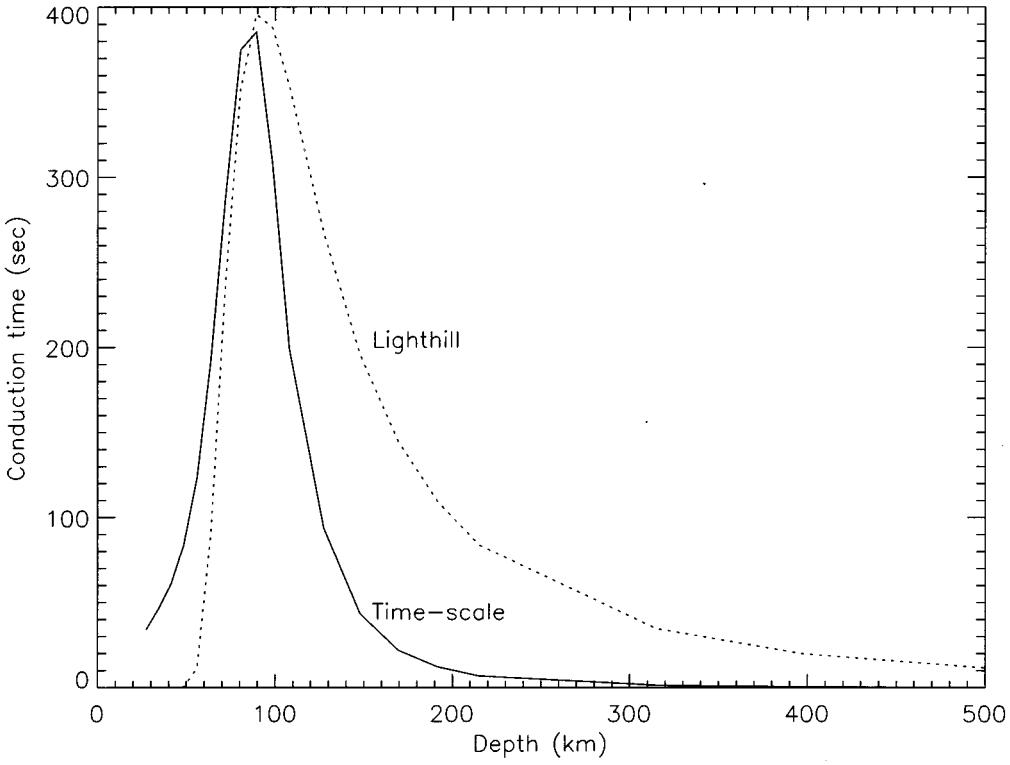

FIG. 7. Solid line: conduction (radiation) time scale in a solar model as a function of depth [21]; dotted line, acoustic flux emitted by convection (arbitrary units).

low states? The answer will be ''the radiative time scale'' $\tau_{\rm rad}$. For a parcel of material of diameter L and opacity χ ($\rm cm^{-1}$), the value of $\tau_{\rm rad}$ is given by [22]

$$\tau_{\rm rad}=\tau_{\rm thin}[1-\chi L\ \cot^{-1}(\chi L)]^{-1}, \tag{10}$$

where

$$\tau_{\rm thin}=\rho C_v/16\chi\sigma T^3. \tag{11}$$

Here σ is the Stefan-Boltzmann constant and C_v is the specific heat at constant volume. Since convective cell sizes in a compressible medium have dimensions comparable to H_p [8,9], it seems appropriate to set $L=H_p$. We evaluate the above expression in a model of the solar convection zone [23] and present the results in Fig. 7. The solid curve shows $\tau_{\rm rad}$ (which, for purposes of comparison with the above discussion, we refer to as $\tau_{\rm cond}$) as a function of depth beneath the level where $T=5800$ K. The radiative time scale tends towards small values near the surface and at great depths. At intermediate depths ($d\approx100$ km), $\tau_{\rm cond}$ reaches a maximum value of 300–400 sec in this model. According to our interpretation of cyclic behavior, this means that convection in the sun at depths of order 100 km is cycling back and forth between high and low states on time scales of 300–400 sec.

To see the significance of this in the solar context, the dotted curve in Fig. 7 indicates the depth dependence of the flux of acoustic power $F_{\rm ac}$ (in arbitrary units), which is created by quadrupole terms in the convective Reynolds stresses [24]: $F_{\rm ac}\sim\rho M^3 v^5$, where v is the convective speed and M is the Mach number. Note that the acoustic flux is sharply peaked at depths of order 100 km and the magnitude of the flux is extremely sensitive to variations in the convective flows: the results in Fig. 7 refer to the mean values in the solar model [23]. In view of the great sensitivity of acoustic emission to v, we suggest that since the convective flux at depths of about 100 km is cycling back and forth on periods of 300–400 sec, this should contribute to significant periodicity in solar acoustic power on periods of the same order. In fact, it has long been known that acoustic modes in the sun are readily detectable at periods around 5 min: the energy per mode peaks at a frequency of about 3 mHz, with a full width at half maximum of 2.8–3.5 mHz [25], i.e., the acoustic emission peaks at periods of 290–360 sec. The overlap between this range and the cycling time that we have found for solar convection suggests that perturbations in the convective flux may be a significant excitation mechanism for solar acoustic modes.

V. CONCLUSION

We have performed two-dimensional simulations of compressible convection in an unstable layer that is sandwiched between stable layers. In a carefully controlled comparison, we have also simulated compressible convection in a single unstable layer in contact with impenetrable walls.

We find (in agreement with previous work) that convective flows in the single-layer case can reach a steady state when the layer is driven moderately supercritical. However, in contrast to this, we find that when the sandwich case is driven with identical strength, the convective flows do *not* reach steady state: instead, they are cyclic. The essential distinction between the single-layer case and the sandwich case

is the following: in the single-layer case, convectively unstable fluid *is in direct contact with unstable boundary layers*, whereas in the sandwich case, *there are no such unstable boundary layers*.

The cyclic fluctuations in the convective heat flux F_C in sandwich convection are not small: *F_C varies by factors of 2–3 between minima and maxima*. In the cycles, there is a clear 90° phase shift between F_C and the dynamic Rayleigh number Ra_d.

We argue that the time scale for the cycles is controlled by conductive processes (essentially the Péclet number). We also argue that the value of Ra_d cycles above and below a limiting mean value Ra_{dm}, which has the following property: the convective growth time scale in fluid that is being driven with strength Ra_{dm} is comparable to the conductive time scale.

ACKNOWLEDGMENTS

This research has been supported by NASA under Grant No. NAGW-2456 through the Astrophysical Theory Program and Grant No. NAG5-1573 through the Space Physics Theory Program. We thank Chang-Hua Tsao for help in various aspects of the computations. The computations were performed on the CRAY-C90 supercomputer at the San Diego Supercomputer Center.

[1] Lord Rayleigh, Philos. Mag. Ser. 6 **32**, 529 (1916).
[2] M. Benard, Rev. Gen. Sci. **12**, 1261 (1900); **12**, 1309 (1900).
[3] E. A. Spiegel, Astrophys. J. **141**, 1068 (1965).
[4] E. A. Spiegel, Astrophys. J. **139**, 959 (1964).
[5] E. Graham, J. Fluid Mech. **70**, 689 (1975).
[6] F. H. Busse, in *Hydrodynamic Instabilities and the Transition to Turbulence*, edited by H. L. Swinney and J. P. Gollub (Springer-Verlag, Berlin, 1985), p. 116.
[7] F. Cattaneo, N. H. Brummell, J. Toomre, A. Malagoli, and N. E. Hurlburt, Astrophys. J. **370**, 282 (1991).
[8] M. Hossain and D. J. Mullan, Astrophys. J. Lett **354**, L33 (1990).
[9] M. Hossain and D. J. Mullan, Astrophys. J. **380**, 631 (1991); **397**, 250 (1992).
[10] N. E. Hurlburt, J. Toomre, and J. M. Massaguer, Astrophys. J. **282**, 557 (1984).
[11] D. Porter and P. Woodward, Astrophys. J. Suppl. **93**, 309 (1994).
[12] Q. Q. Cheng, M. Hossain, and D. J. Mullan, Astrophys. J. **444**, 789 (1995).
[13] N. E. Hurlburt, J. Toomre, and J. M. Massaguer, Astrophys. J. **311**, 563 (1986).
[14] N. E. Hurlburt, J. Toomre, J. M. Massaguer, and J.-P. Zahn, Astrophys. J. **421**, 245 (1994).
[15] O. Andreasson, B. N. Andersen, and C. E. Wasberg, Astron. Astrophys. **257**, 763 (1992).
[16] H. Muthsam *et al.*, Astron. Astrophys. **293**, 127 (1995).
[17] M. Hossain and D. J. Mullan, Astrophys. J. **416**, 733 (1993).
[18] K. L. Chan and D. Gigas, D. Astrophys. J. Lett. **389**, L87 (1992).
[19] B. Castaing *et al.*, J. Fluid Mech. **204**, 1 (1989).
[20] A. Belmonte, A. Tilgner, and A. Libchaber, Phys. Rev. E **51**, 5681 (1995).
[21] P. V. Foukal, *Solar Astrophysics* (Interscience, New York, 1990), p. 458.
[22] E. A. Spiegel, Astrophys. J. **126**, 202 (1957).
[23] N. Baker and S. Temesvary, *Tables of Convective Stellar Envelopes* (Goddard Institute of Space Studies, New York, 1966).
[24] L. Biermann and R. Lust, in *Stellar Atmospheres*, edited by J. Greenstein (University of Chicago Press, Chicago, 1960), p. 272.
[25] K. Libbrecht, Astrophys. J. **334**, 510 (1988).